Inhalation Toxicology, 19:1045–1054, 2007

ISSN: 0895-8378 print / 1091-7691 online
DOI: 10.1080/08958370701626501

informa
healthcare

Deposition of Ultrafine (NANO) Particles in the Human Lung

Bahman Asgharian and Owen T. Price
The Hamner Institutes for Health Sciences, Research Triangle Park, North Carolina, USA

Increased production of industrial devices constructed with nanostructured materials raises the possibility of environmental and occupational human exposure with consequent adverse health effects. Ultrafine (nano) particles are suspected of having increased toxicity due to their size characteristics that serve as carrier transports. For this reason, it is critical to refine and improve existing deposition models in the nano-size range. A mathematical model of nanoparticle transport by airflow convection, axial diffusion, and convective mixing (dispersion) was developed in realistic stochastically generated asymmetric human lung geometries. The cross-sectional averaged convective-diffusion equation was solved analytically to find closed-form solutions for particle concentration and losses per lung airway. Airway losses were combined to find lobar, regional, and total lung deposition. Axial transport by diffusion and dispersion was found to have an effect on particle deposition. The primary impact was in the pulmonary region of the lung for particles larger than 10 nm in diameter. Particles below 10 nm in diameter were effectively removed from the inhaled air in the tracheobronchial region with little or no penetration into the pulmonary region. Significant variation in deposition was observed when different asymmetric lung geometries were used. Lobar deposition was found to be highest in the left lower lobe. Good agreement was found between predicted depositions of ultrafine (nano) particles with measurements in the literature. The approach used in the proposed model is recommended for more realistic assessment of regional deposition of diffusion-dominated particles in the lung, as it provides a means to more accurately relate exposure and dose to lung injury and other biological responses.

Ultrafine (nano) particles are ubiquitous in ambient particulate pollution (Riesenfeld et al., 2000). Increased availability of products manufactured from nanomaterial increases the possibility of exposure to airborne nanomaterials. Once inhaled, nanoparticles have a high probability of deposition in the lung due to their small size. This deposition occurs primarily by diffusion and secondarily by thermophoretic effects in the first few airways of the lung during exhalation. Exposure to nanoparticles can exacerbate respiratory disease (Peters et al., 1997) and produces toxicity even at low concentrations (Johnston et al., 2000). Studies from accidental exposure to heating plastic materials such as Teflon have shown high pulmonary (PUL) toxicity in humans (Makulova, 1965; Rosenstock & Cullen, 1986). Laboratory inhalation studies in rats indicate that toxic effects are related to the ultrafine, nanosized fraction of the products (Ferin & Oberdörster, 1992; Oberdörster et al., 1992). Nanosized particles induce more intense airway inflammation than similar mass concentrations of larger particles (Oberdörster et al., 1995).

Due to their physicochemical characteristics that give them enhanced properties (Maynard et al., 2004), manufactured nanoparticles may be biopersistant and remain intact and cause toxicity. In addition, toxicity may depend on internal structure and particle size, so that the particle acts as a carrier transport to carry material into the lung (Johnston et al., 2000). High particle number, overall large surface areas, and high lung deposition efficiency may also be important in contributing to the health effects (Oberdorster et al., 1995; Utell & Frampton, 2000).

Because of potential toxic effects, it is critical to have a realistic assessment of the regional deposition of nanoparticles in the lung. Mathematical models have been developed to predict deposition of inhaled particles in the lungs of humans and animals. There are many deposition models available that are either empirical in nature (Rudolf et al., 1986, 1990), compartmental (ICRP, 1994; NCRP, 1997), or continuous (i.e., mechanistic), based on physics of airflow and particle transport (Yu, 1978a). In addition, mechanistic models may be deterministic

Received 22 May 2007; accepted 25 July 2007.
This study was supported in part by the EPA STAR grant RD 832531-01-0 and the Long Range Research Initiative (LRI) of American Chemistry Council (ACC).
Address correspondence to Bahman Asgharian, Associate Investigator, The Hamner Institutes for Health Sciences Durham, NC 27709, USA. E-mail: Asgharian@thehamner.org

(Anjilvel & Asgharian, 1995; Asgharian et al., 2001) or probabilistic (Hofmann & Koblinger, 1990; Koblinger & Hofmann, 1990).

The applicability of existing mechanistic models in the nanosize range may be limited because nanoparticle-specific mechanisms of transport and deposition were not fully implemented. While the transport equation may have included axial diffusion to determine penetration though lung airways, wall loss calculations have often excluded the influence of axial diffusion on lateral movement of nanoparticles toward airway walls (e.g., Taulbee et al., 1978). The exclusion was based on the observation that axial diffusion has a negligible effect on deposition when the Peclet number is over 200 (Tan & Hsu, 1971). In addition, airflow in the upper airways is complex and the presence of turbulence and secondary flows at the bifurcation may impact particle losses. In fact, measurements of ultrafine particle deposition in tracheobronchial (TB) airways of lung casts have indicated at least a twofold increase in deposition compared with available predictions models (Cohen et al., 1990; Cohen & Asgharian, 1990). Given that diffusion losses of nanoparticles in the upper airways of the lung are significant (see Results section), a more accurate assessment of diffusion losses in the upper airways of the lung is necessary.

In addition to axial diffusion, dispersion of particles (of all sizes) by convective mixing will cause a migration of particles from the tidal air to the residual air. Dispersion due to convective mixing has been attributed to various mechanisms such as Taylor dispersion when axial and radial motion are comparable, asynchronous and inhomogeneous ventilation (as in diseased 70 lungs), disturbances and secondary motions at the bifurcations, irreversibility of flow between inhalation and exhalation, and mixing in the alveoli (Taulbee et al., 1978; Yu, 1978b). Convective mixing has often been assumed to be diffusive in nature, propagating by dispersion (Darquenne et al., 1997; Edwards, 1994; Egan et al., 1989; Hofmann et al., 1994; Taulbee & Yu, 1975). Gas dispersion models have often been used in particle deposition models to assess particle losses (e.g., Taulbee & Yu, 1978; Darquenne & Paivia, 1994). Use of gas dispersion models will exaggerate particle dispersion because gases have a significantly higher diffusivity than particles. Recently, Lee et al. (2000) and Lee and Lee (2001) conducted a numerical study of particle transport through a double-bifurcated airway system and showed that axial streaming was mainly responsible for particle dispersion in conducting airways and the use of a gas dispersion model to estimate particle dispersion overestimated mixing of particles by as much as 35% during inhalation and 30% during exhalation. Following the steps of the experimental study by Scherer et al. (1975), these investigators developed dispersion models for particles.

In addition to dispersion by axial streaming in conducting airways, there is additional mixing in the PUL region. Recent studies suggest that PUL mixing may be due to chaotic advection (Henry & Tsuda, 2002; Henry et al., 1999; Tsuda et al., 1995, 1999). Despite strong evidence based on numerical studies and laboratory testing in physical models, there is a lack of experimental observation in humans on the chaotic nature of mixing (Darquenne & Prisk, 2004). Due to high diffusive losses of nanoparticles in the tracheobronchial region, PUL mixing may be secondary and negligible. Hence only dispersion by axial streaming was included in the current model.

Failing to include a realistic account of particle dispersion, existing mechanistic deposition models also face a computational limitation. In these studies, the governing transport equations have been solved numerically by a finite-difference scheme that required extensive computation times. In practice, numerical computations could only be performed in typical-path lung geometries. The use of a typical-path lung geometry is reasonable for average deposition estimates because the lung geometry is based on averaged lung dimensions per generation. However, no information on subregional (i.e., lobar etc.) deposition or the distribution of deposited particles throughout the lung can be obtained.

In this study, an existing model of particle deposition (Asgharian et al., 2001) developed for any lung geometry was refined for ultrafine (nano) particles. This was achieved by using improved models of particle losses by diffusion and including particle-specific axial diffusion and dispersion effects in the transport equation. An analytical solution to the particle transport equation was found that allowed fast computation of particle concentration and deposition per airway. Deposition calculations of nanosized particles were performed in a number of asymmetric lung geometries to provide a range of deposition for particles of varying sizes in people. Deposition model for nanoparticles was tested by comparing the predictions against available measurements in the lung and TB and PUL regions.

LUNG GEOMETRY

Based on morphometric measurements of Raabe et al. (1976), Koblinger and Hofmann (1985) developed functional relationships for airway parameters such as length, diameter, branching angle, cross-sectional area of the daughter branches, gravity angle, and correlations between these parameters as a function of airway generation number. These functional relationships were used to create stochastic lung geometries for the human lungs (Koblinger & Hofmann, 1990). Thirty such geometries were constructed and used for deposition calculations. These lung geometries were based on the same structural relationship, varying primarily in their conducting airway volumes.

MODELING TRANSPORT AND DEPOSITION OF NANOPARTICLES IN THE LUNG

Transport of nanoparticles in the respiratory tract occurs by convective movement in the upper airways of the lung where particles are carried into the lung by the inhaled air and by random walk from the tidal air to the reserve air in the lower airways where airflow momentum is practically diminished. Random walk by diffusion is a unique feature of nanoparticles and is

absent for fine and coarse particles. Particle deposition modeling in the respiratory tract consists of tracking inhaled particles during a breathing cycle that is made up of the three phases of inhalation, pause, and exhalation, and determining the fraction of inhaled particles that reach and deposit in various locations of the lung. Several assumptions are made in the calculation of particle losses. First, it is assumed that the lung expands and contracts uniformly during breathing. Second, the tidal air travels through the lung with a uniform velocity that is equal to the average velocity of a parabolic flow with the same flow rate. Third, axial diffusion of particles within the tidal air is negligible but depending on circumstances there may be a significant diffusive transport of particles across the tidal air to the reserve air. In addition, particles are monodisperse and uncharged. Because of the enormity of the number of airways, uncertainties regarding true airway geometry and lung ventilation, and limitations in calculating the flow field for the entire respiratory tract, precise numerical solution of nonlinear transport equations are prohibitive and unnecessary. Instead, the movement of particles in lung airways can be described by the simplified, cross-sectional area averaged, convective-diffusion equation:

$$\frac{\partial(AC)}{\partial t} + \frac{\partial(QC)}{\partial x} = \frac{\partial}{\partial x}\left(DA\frac{\partial C}{\partial x}\right) - \lambda AC \qquad [1]$$

where A is the total airway cross-sectional area and includes the contribution of the alveoli surrounding the airways in the PUL region, C is the particle concentration, D is the apparent diffusion coefficient, Q is the flow rate through the airway, λC is the number of particles lost to the airways by diffusion per unit time, per unit volume, and $x$and t are the distance into the lung and elapsed time, respectively. Apparent diffusion coefficient D is the sum of molecular diffusion coefficient (D_m) and effective diffusion coefficient (D_e) by dispersion. Scherer et al. (1975) measured the spreading of a bolus of benzene vapor in five-generation, bifurcating glass tubes and calculated the effective diffusion coefficient. Since convective mixing (dispersion) depends on the Peclet number. which in turn is related to airway diameter and mean axial velocity of the flow, the following semiempirical relationship was proposed for the effective diffusion coefficient:

$$D_e = 2\gamma U R_0 \qquad [2]$$

in which U is the airflow velocity and R_0 is the airway radius. Scherer et al. (1975) found coefficient $\gamma = 1.08$ for inhalation and $\gamma = 0.37$ for exhalation by fitting Eq. (2) to calculated effective diffusion coefficients. Axial dispersion described by Eq. (2) becomes negligible in the PUL airways because of diminishing airflow velocity and particle transport is mainly by molecular diffusion. Due to the lack of data, Eq. (2) and other similar equations have been extended to particles (Darquenne & Paiva, 1994; Hofmann et al., 1994; Taulbee & Yu, 1978) despite being specifically developed for gases. Because of having a higher diffusivity, particles supposedly will penetrate deeper than expected into the lung by axial dispersion. Hence, upper airway deposition will be underestimated and lower airway deposition will be overestimated. Experiments on particle dispersion are not available to date. However, there have been numerical studies duplicating the experiments of Scherer et al. (1975) for particles. Lee et al. (2000) computed airflow particle transport in a double bifurcation airway system for the case of inhalation and found $\gamma = 7.0$ when dispersion was represented by Eq. (2). Similarly, Lee and Lee (2001) found $\gamma = 26.0$ for exhalation. Due to the lack of experimentally based data for particles, values of γ numerically obtained by Lee et al. (2000) and Lee and Lee (2001) were selected and used in this study.

The sink term, λC, in Eq. (1) alleviates the need to specify boundary conditions along airway walls. The flux term, λ, is related to particle deposition efficiency, which is the fraction of entering particles that deposit in an airway:

$$\eta = \int \lambda dt \qquad [3]$$

Nanoparticle deposition in lung airways occurs primarily by diffusion. Tan and Hsu (1971) computed and tabulated deposition efficiency of particles traveling in a cylindrical tube by a fully developed laminar (parabolic) flow in the presence of axial diffusion. Deposition efficiency was found to be related to two nondimensional parameters, *Pe* and Δ. The Peclet number, $Pe = 2UR_0/D_m$, is the ratio of convective to diffusive transport of particles, and the nondimensional parameter, $\Delta = D_m L/4UR_0^2$ where L is the airway length, represents the ratio of diffusion time scale of particles across the airway to average residence time of parlicles inside the airway due to flow convection. To obtain an analytical form of the deposition equation for use in Eq. (1), a functional relationship between deposition efficiency, η, and nondimensional parameters Δ and *Pe* was adopted:

$$\eta = 1 - e^{-a\Delta^b} \qquad [4]$$

where constant coefficients a and b in Eq. (4) were found by fitting the equation to the tabulated data of Tan and Hsu (1971). Values for coefficients a and b are given in Table 1 for different

TABLE 1
Coefficients a and b in equation (4) for selected values of Peclet number

Pe	a	b
1	3.7122	0.92229
5	10.7	0.92918
10	11.546	0.88166
50	10.36	0.79556
100	9.8986	0.77719
$\propto$	9.5768	0.77719 (no axial diffusion)

Pe values. Equation (4) is based, on the transport of small size particles by diffusion in a straight cylindrical tube. While it can be used to compute deposition efficiency of particles by diffusion in most airways of the lung for which the flow is fully developed and laminar, it may not be adequate for use in the most upper airways of the lung because of the presence of turbulence and mixing at the bifurcations. Mathematical equations predicting particle losses by diffusion in upper airways of the lung have not been developed in part due to the complexity of airflow structure and particle transport. However, there are measurements of ultrafine particle deposition in conducting airways of human casts (Cohen et al., 1990). Cohen and Asgharian (1990) used the measurements to develop a semi-empirical relationship between deposition efficiency and non-dimensional, parameters Δ and *Pe*. They found that dependence on *Pe* was weak and deposition efficiency was related to Δ by:

$$\eta = 2.965\Delta^{0.568} \quad [5]$$

This equation was used for the upper most airways of the lung ($L/(R_0 \cdot Re) < 10^{-3}$, where *Re* is the Reynolds number) to calculate deposition efficiency by diffusion. Otherwise Eq. (4) was used. It should also be noted that Eqs. (4) and (5) converge when $L/(R_0 \cdot Re) > 10^{-3}$ (Cohen Asgharian, 1990).

The species transport and deposition model presented by Eq. (1) is common in calculating gas-uptake (Chang & Farhi, 1973; Davidson, 1981; Miller et al., 1985; Overton, 2001; Overton et al., 2001; Pack et al., 1977; Tawhai & Hunter, 2001; Yu, 1975) and particle deposition (Darquenne & Paiva, 1994; Hashish, 1992; Nixon & Egan, 1987; Taulbee & Yu, 1975; Taulbee et al., 1978; Yu, 1978a, b). While Eq. (1) is often solved numerically, an analytical solution is also possible. For a uniformly expanding and contracting airway, conservation of inhaled mass yields (Yu, 1978a):

$$\frac{\partial A}{\partial t} = -\frac{\partial Q}{\partial x} \quad [6]$$

Expanding Eq. (1), substituting for $\partial A/\partial t$ from Eq. (6) and setting $\partial A/\partial x = 0$ because airways are assumed to be cylindrical, the following equation will be obtained:

$$\frac{\partial C}{\partial t} + \frac{Q}{A}\frac{\partial C}{\partial x} = D\frac{\partial^2 C}{\partial x} - \lambda C \quad [7]$$

Eq. (7) can be solved within the tidal air by neglecting the diffusive term by assumption (Yu, 1978a). A solution of Eq. (7) retaining the diffusive term using the initial and boundary conditions of

$$\begin{cases} \text{At} \quad t = t_0 \quad \text{and} \quad 0 \le x \le \infty, & C = 0 \\ \text{At} \quad t > t_0 \quad \text{and} \quad x \le x_f, & C = C_f = C_0 e^{-\lambda_f (t-t_0)} \\ \text{At} \quad t > t_0 \quad \text{and} \quad x = \infty, & C = 0 \end{cases} \quad [8]$$

can be given in terms of the complementary error function:

$$C(x,t) = C_0 e^{-\lambda(t-t_0)}\text{erfc}\left(\frac{x - x_f}{2\sqrt{D(t-t_0)}}\right) \cong C_0(1-\eta_f)(1-\eta_d)\text{erfc}\left(\frac{x - x_f}{2\sqrt{D(t-t_0)}}\right) \quad [9]$$

where C_0 and t_0 are the concentration and elapsed time at the entrance to the airway respectively, C_f is the aerosol front concentration, λ_f is losses per unit time per unit volume in the tidal air, η_f denotes the deposition efficiency in the section of the airway occupied by the tidal air, η_d is the deposition efficiency of particles in the remaining section of the airway in the residual air distal to the tidal air, and $x_f = \int_{t_0}^{t}(Q/A)dt$ denotes the front location (leading edge of the tidal air) (Anjilvel and Asgharian, 1995). Thus, Eq. (9) gives average particle concentration in an airway at location x ahead of the tidal air and can be used to calculate particle losses in the portion of the residual air that is not mixing with the tidal air by convection. Equation (9) is the first analytical model that uses the diffusive transport of particles in addition to the convective transport to calculate concentration and deposition of nanosized particles. Equation (9) is valid for steady breathing only. However, it is applicable to normal breathing scenarios for which the flow inertia due to cyclic breathing is negligible. Equation (9) provides an advantage over existing computational models. Since a realistic lung geometry is key in accurate prediction of particle deposition in the lung (Asgharian et al., 2004), typical-path models are reliable only for the calculation of average regional deposition (Asgharian et al., 2001). The computation time of models that solve some form of Eq. (7) numerically (e.g., Taulbee et al., 1978; Darquenne & Paiva, 1994) is fairly large, prohibitive for asymmetric lung geometry, and in practice only useful for typical-path lung geometries. It is difficult to extend these models to more complete and realistic lung geometries. The model presented by Eq. (9) can be applied to asymmetric lung geometries of many thousands of conducting airways (plus many additional PUL airways) to study distribution of the deposited particles among various airways of the lung.

Equation (9) can be used to find particle concentration ahead of the front at an end of the airway before the tidal air reaches the end during inhalation and after the tidal air recedes during exhalation. Losses by diffusion ahead of the front in an airway is calculated from

$$\text{Losses} = \int\int \lambda_d C A dx dt \quad [10]$$

Assuming a linear variation of particle concentration in the airway, Eq. (10) will take on the following form during inhalation:

$$\text{Losses} = \eta_d Q\left[\int_{t_0}^{t_{\text{prox}}} \frac{C_{\text{prox}}(t) + C_{\text{dist}}(t)}{2} dt + \int_{t_{\text{prox}}}^{t_{\text{dist}}} \frac{C_f(t) + C_{\text{dist}}(t)}{2}\left(1 - \frac{x_f(t)}{L}\right) dt\right] \quad [11]$$

where t_{prox} is the time for the front to reach the proximal end of the airway. t_{dist} is the time it takes for the aerosol front to reach the distal end of the airway, and C_{prox} and C_{dist} are aerosol concentrations at the proximal and distal ends of the airway respectively. The first term within the bracket on the right hand side of Eq. (11) corresponds to losses before the tidal air (front) reaches the airway and the second term corresponds to losses when the front is crossing the airway. Similarly, losses during exhalation are represented by

$$\text{Losses} = \eta_d Q \left[\int_{t_{dist}}^{t_{prox}} \frac{C_f(t) + C_{dist}(t)}{2} \left(1 - \frac{x_f(t)}{L}\right) \text{dt} + \int_{t_{prox}}^{T} \frac{C_{prox}(t) + C_{dist}(t)}{2} \text{dt} \right] \quad [12]$$

where T corresponds to the breathing period. The first term in Eq. (12) represents losses while the front is retreating from the airway and the second term denotes airway losses in the airway thereafter until the end of the breathing cycle. Airway losses during inhalation and exhalation were combined for various airways to find deposition per region, lobe, and total lung deposition.

RESULTS AND DISCUSSION

Penetration and deposition of particles from 1 nm to 100 nm were calculated in asymmetric (stochastic) morphometric models of the human lung (Koblinger & Hofmann, 1990) with and without the presence of diffusive transport of particles in the lung. For the case of no axial diffusion or dispersion, the deposition model developed earlier by Asgharian et al. (2001) was employed. Two lung geometries were selected from a pool of 30 stochastically created geometries that corresponded to lungs with the smallest and largest number of bronchial airways. These are referred to as small bronchial airway number (SBAN) and large bronchial airway number (LBAN) in this article. Since PUL volumes were identical among all lung geometries, deposition calculations in these limiting geometries provided the bound for the predictions. Deposition calculations were performed at a lung functional residual capacity (FRC) of 3300 ml with a tidal volume of 625 ml. A breathing frequency of 12 breaths per minute (minute ventilation of 7500 ml) with equal breathing time during inhalation and exhalation and no pause were selected for the computations. Particle deposition calculations were performed at a lung volume midway between the lung at rest (FRC) and end of inhalation (i.e., at FRC + half the tidal volume). To study lung filtering capability and distribution of the deposited particles among airways, particles were assumed to bypass the head airways and enter the lung via the trachea. The head filtering has to be included when assessing the lung dose as a function of particle size. The significance of axial diffusion depends on the strength of the convective transport of particles. In the upper airways of the lung, flow convection is strong and little axial diffusion is expected. The opposite is true in the deep lung, where flow convection has practically diminished to zero and particle penetration is primarily by axial diffusion in the absence of dispersion. Tan and Hsu (1971) found that for particle transport in a fully developed parabolic flow, axial diffusion can be neglected if Pe $\geq$ 200. To examine the significance of axial transport by diffusion, Peclet number is plotted in Figure 1 as a function of airway generation number for particles in the size range of 1 nm to 1 μm. Due to strong flow convection, axial diffusion is negligible for all particle sizes in the first seven generations of the lung. Beyond generation 8, particle penetration by diffusion is significant for particles smaller than 10 nm. Diffusive penetration in the lung becomes progressively smaller for particles between 10 nm and 0.1 μm. For particles larger than 0.1 μm, axial transport by diffusion is essentially zero. To further investigate the penetration depth of different size nanoparticles, normalized concentrations of 1-nm, 5-nm, and 10-nm particles were calculated at the end of inhalation. Normalized concentration was defined as the ratio of concentration at any location divided by the concentration at the inlet to the trachea. The results are shown in Figure 2. There was no penetration of 1-nm particles beyond generation 11 due to high deposition in the preceding airways. As particle size increased, losses by diffusion decreased and as a result, particle penetration into the lung increased. While there was little penetration of

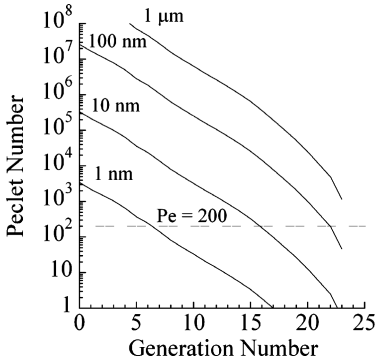

FIG. 1. Calculated Peclet number (Pe) in airway generations of the human lung for a lung tidal volume of 625 ml and breathing frequency of 12 breaths per minute.

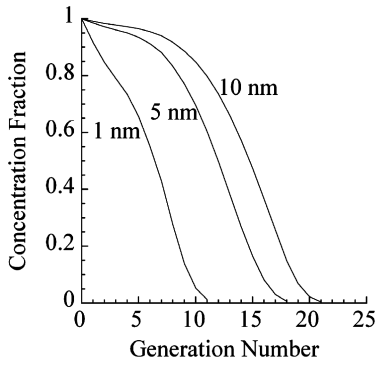

FIG. 2. Concentration of inhaled 1-, 5-, and 10-nm nanoparticles in the lung at the end of inhalation for breathing via the trachea.

5-nm particles, a significant portion of 10-nm particles reached the PUL region. The results presented in Figure 2 correspond to breathing via trachea. The penetration is even more limited than that shown in Figure 2 if losses in the head region are accounted for. The inability of nanoparticles less than 5 nm in size to reach the P UL airways limits the effects of axial diffusion and dispersion on particle deposition in the deep lung. In order to develop a simple and mathematically manageable theoretical model, a number of deposition modeling efforts have neglected axial diffusion and dispersion (Anjilvel & Asgharian, 1995; Asgharian et al., 2001; Hofmann & Koblinger, 1990; Yu, 1978a; and others). To examine the influence of axial diffusion and dispersion on deposition and its significance on deposition of nanoparticles in particular, deposition fractions of particles between 1 nm and 100 nm were calculated in different regions of the human lung for the cases of particle penetration by convection and convection plus diffusion and dispersion. Figure 3 A and B, shows predicted deposition fractions in the SBAN and LBAN stochastic lungs, respectively. Diffusive transport of particles through lung airways has no effect on particle deposition in the TB region of the SBAN stochastic lung (Figure 3A) but a small increase is noticed for particles below 10 nm in the LBAN stochastic lung (Figure 3B). This is because flow convection is much stronger than axial diffusion for particles larger than 1 nm in TB airways as shown by Peclet number values over 200 in Figure 1. The most significant but limited effect on deposition by including diffusion and dispersion is observed in the PUL region of both lung geometries for particles greater than 10 nm. Because of diminishing airflow velocity, convective mixing [Eq. (2)] becomes negligible in the PUL region. Axial diffusion will cause additional transport and deposition of particles in the PUL region. However, flow convection is still larger than axial diffusion except in the alveolar sacs (very last airway generation). Hence, the contribution to particle losses in the PUL region from diffusive transport is smaller than that due to convective transport. The increase in PUL deposition may vary between 5% and 10% depending on particle size and lung geometry. As a result of the increase in PUL deposition, lung deposition is also increased by a few percent. Particle penetration and deposition in the lung is the interaction of convective transport and axial diffusion plus dispersion. Both processes are affected by breathing pattern. Model predictions presented in Figure 3 were based on the default breathing pattern of a lung tidal volume of 625 ml and a breathing pattern of 12 breaths per minute. To examine the effect of breathing pattern on deposition by each transport mechanism, two other breathing maneuvers were simulated: fast shallow breathing represented by a tidal volume of 250 ml and a breathing frequency of 30 breaths per minute and slow deep breathing represented by a tidal volume of 1500 ml and a breathing frequency of 5 breaths per minute. The minute volumes in both cases were kept at 7.5 lpm. Figure 4 A and B, gives predicted regional deposition fraction in the SBAN stochastic lung. Similar findings are observed in the LBAN stochastic lung and hence those results are not given here. Changes in breathing patterns exert more influence on deposition from convective flow than that from axial diffusion and dispersion. Slow deep breathing causes a significant increase in both TB and PUL deposition. Shallow fast breathing causes a drop in PUL deposition of more than 30%. There are virtually no changes in TB deposition for both breathing maneuvers when axial diffusion and dispersion are included. The only change in deposition occurs in the PUL region. Losses contributed to diffusive transport are clearly more significant in the fast shallow breathing than in slow deep breathing. However, the difference in deposition is below 10% as in the case of default breathing with the same minute ventilation (Figure 3). An advantage of stochastically generated lung geometries is that inter- and intrasubject variability can be examined by calculating deposition of particles in many lung geometries. Figure 5 shows deposition in the TB and PUL regions of 30 such geometries. Deposition variations in both regions are small near 1-nm and 100-nm size particles. This is because of very high and very low particle deposition for 1-nm and 100-nm particles, respectively. The largest variation in deposition is for 10-nm-diameter particles for which the diffusion mechanism is neither overwhelming nor insignificant. By the same argument, a wide range of particle deposition is observed in the PUL region.

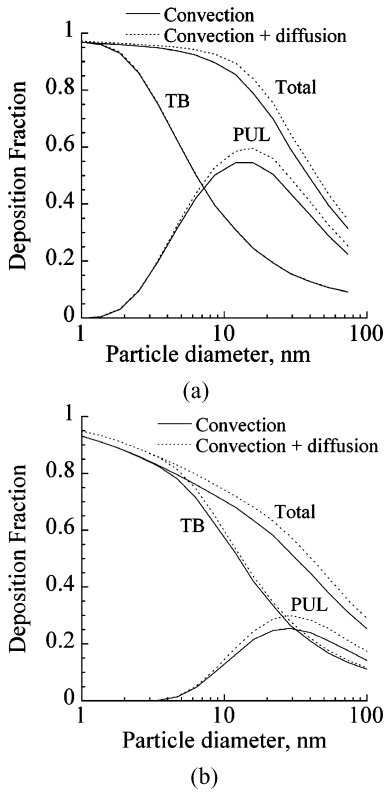

FIG. 3. Regional deposition fraction of inhaled particles in the SBAN and LBAN stochastic human lungs for a lung tidal volume of 625 ml, breathing frequency of 12 breaths per minute, and breathing via the trachea. (A) SBAN stochastic lung geometry; (B) LBAN stochastic lung geometry.

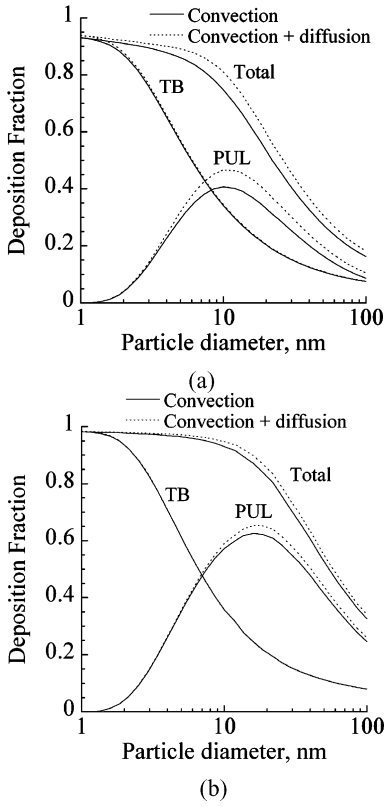

FIG. 4. Regional deposition fraction of inhaled particles in the SBAN stochastic human lung geometry. (A) Shallow fast breathing. (B) Deep slow breathing.

Because of the differences in TB deposition, the peak PUL deposition, which is due to TB filtering effects, is observed at a different particle size for each lung geometry. Deposition of particles between 1 nm and 100 nm in the left upper (LU), left lower (LL), right upper (RU), right middle (RM), and right lower (RL) lobes are shown in Figure 6 A–C. Deposition in the LL and RU lobes was higher than that in other lobes. Consequently, deposition in the RL and LU lobes that have similar lobar volumes is reduced. The RM lobe, which has the smallest lobar volume, has the least deposition of particles. It is interesting to note that despite having the highest deposition values, variation of deposition per particle size in the LL lobe is small compared with that in other lobes. There is a significant variation of predicted deposition in the right lobes (except for particles larger than 10 nm in the RM lobe) for different stochastic lung geometries.

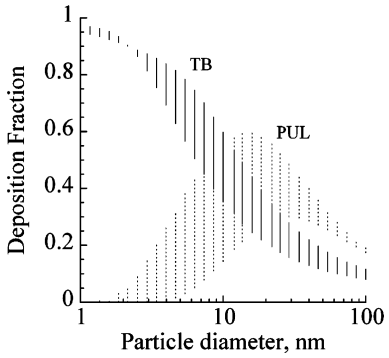

FIG. 5. TB and PUL deposition of particles in 30 stochastically generated human lung geometries for a lung tidal volume of 625 ml, breathing frequency of 12 breaths per minute, and breathing via the trachea.

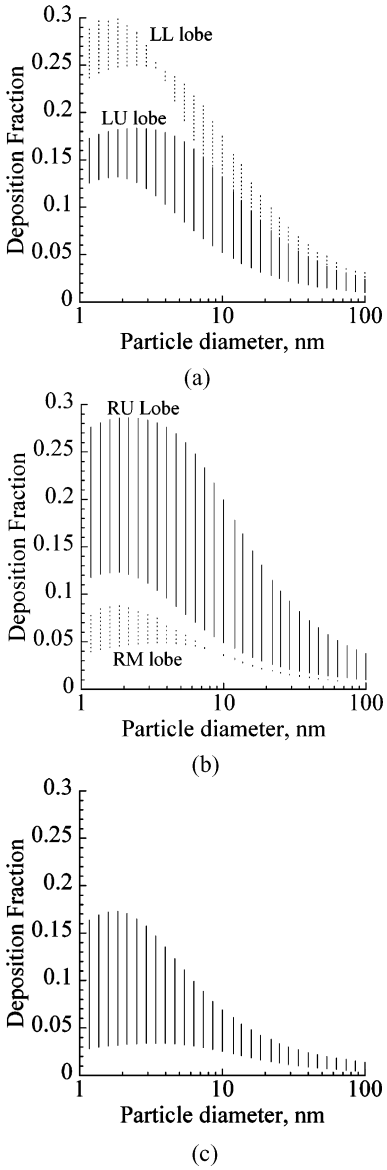

FIG. 6. Lobar deposition of particles in 30 stochastically generated human lungs for a lung tidal volume of 625 ml, breathing frequency of 12 breaths per minute, and breathing via the trachea. (A) Left lobes. (B) Right upper and right middle lobes. (C) Right lower lobe.

Comparison With Available Measurements

A number of studies have reported deposition fraction of small-size particles in the lungs of people. For model confirmation, we selected those studies that had also reported lung functional residual capacity (FRC) and breathing parameters of the subjects as these are key parameters that help determine particle deposition. Deposition comparisons were made for particles between 5 nm and 100 nm. Figure 7 A and B, shows the comparison of predicted total deposition fraction against measurements of Heyder et al. (1986), Jaques and Kim (2000), Schiller et al. (1988), and Tu and Knudson (1984) in the SBAN and LBAN stochastic lungs, respectively. Measurements corresponded to oral breathing and hence predictions were made based on oral route of breathing. Each point in Figure 7, A and B, is the plot of deposition measurement in a different subject or different breathing condition against the predicted value. The appropriate FRC was used for each computation. Also plotted in each figure is the line of identity that corresponds to a perfect match between measurements and predictions. The agreement between predictions and measurements is reasonable in both geometries, although it is much more convincing in the LBAN stochastic lung. The agreement with Heyder et al. (1986) and Tu and Knudson is excellent, while comparison with the measurements of Schiller et al. (1988) shows some scatter around the line of identity for the SBAN stochastic lung. Predictions tend to be slightly higher than measurements of Jaques and Kim (2000) in both lung geometries. While a number of studies have reported measured total deposition in the lung, information on regional deposition is scarce. A true model confirmation requires data comparison at the regional, lobar, and local (airway) levels. However, limitations in measurement techniques prohibit such endeavors. Recently, Kim and Jaques (2000) measured respiratory deposition of ultrafine particles (40 to 100 nm) in healthy young adults in a series of bolus delivery techniques in which bolus aerosol were delivered to lung depths of 50 ml to 500 ml in 50-ml intervals. Assuming a compartmental model of the lung and defining head, TB, and PUL regions based on lung depth volumes, total deposition measurements were converted to regional deposition fractions. Figure 8 A and B, gives comparisons of model predictions in the TB region with values derived by Kim and Jaques (2000). The agreement between model predictions and reported TB deposition of Kim and Jaques (2000) is reasonable. Model predictions slightly overestimate values of Kim and Jaques (2000) in the SBAN stochastic lung and slightly underestimate the values in the LBAN stochastic lungs. The corresponding comparison for the PUL region is given in Figure 9 A and B. Predicted deposition fractions are noticeably higher than reported values by Kim and Jaques (2000). The difference is even greater for the LBAN stochastic lung. A few observations may be made regarding values obtained by Kim and Jaques (2000). To arrive at regional

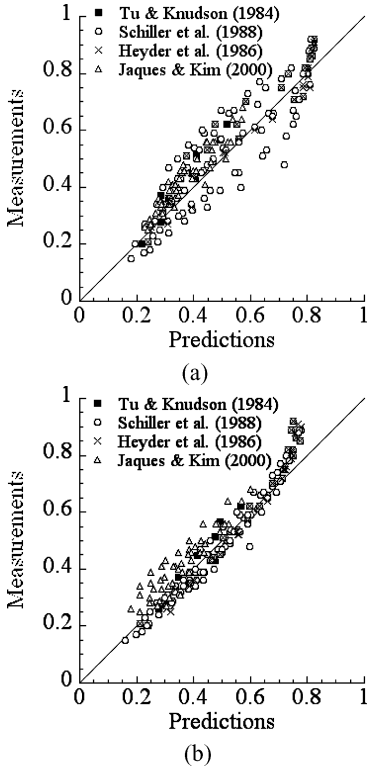

FIG. 7. Comparison of the predicted total deposition of particles with available measurements. (A) SBAN stochastic lung. (B) LBAN stochastic lung.

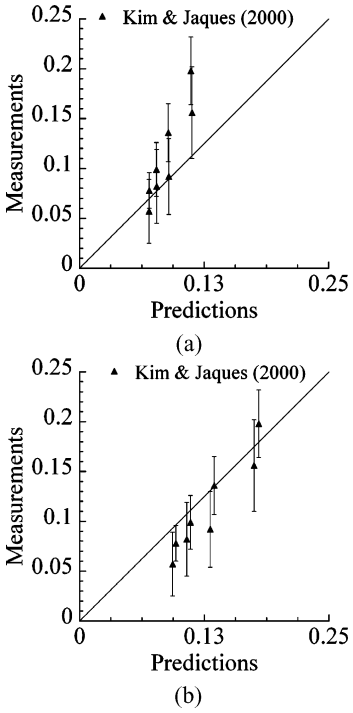

FIG. 8. Comparison of the predicted TB deposition of particles with reported values by Kim and Jaques (2000). (A) SBAN stochastic lung. (B) LBAN stochastic lung.

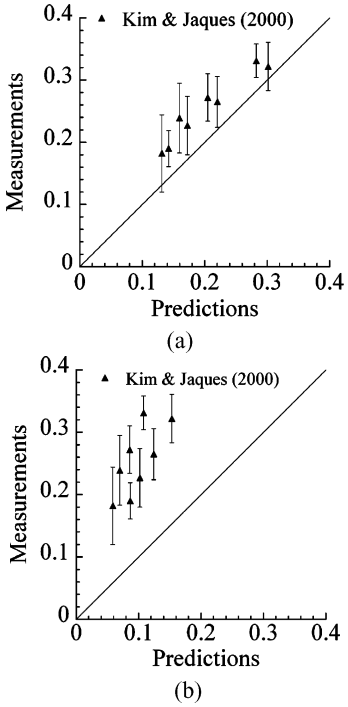

FIG. 9. Comparison of the predicted PUL deposition of particles with reported values by Kim and Jaques (2000). (A) SBAN stochastic lung. (B) LBAN stochastic lung.

deposition fractions, Kim and Jaques (2000) assumed the lung to be symmetric while our analyses are entirely based on more realistic asymmetric lung geometries. They also neglected axial diffusion and convective mixing which is the motivation for this study. In addition, compartmental representation for particle transport made by Kim and Jaques (2000) assumes a steady-state, steady flow of tidal air, which tends to overestimate losses. However, most notably, compartmentalizing the lung based on the volume of inhaled air is not warranted, as a small bolus of inhaled air may travel deep into the lung. For these reasons there are uncertainties associated with experimentally derived values by Kim and Jaques (2000), which may help to explain the discrepancies between our predictions and their reported values.

SUMMARY

An analytical model for the transport of ultrafine (nano) particles in the human lung was obtained by modeling convective flow and axial diffusion and dispersion. Particle deposition fractions in various regions and lobes of the stochastically generated, asymmetric lung geometries were computed. The effects of lung structure and breathing pattern on deposition were investigated with and without the presence of axial diffusion and dispersion. TB deposition was less sensitive to lung structure when compared with PUL deposition. The addition of axial diffusion and dispersion was found to raise predicted deposition in the PUL region up to 10% depending on particle size. A change in breathing pattern affected deposition from the convective flow much more than that from axial diffusion and dispersion. Deposition of nanoparticles smaller than 5 nm was high in the TB region. As a result, very few particles reached the alveolar airways to be available for deposition. Deposition in the alveolar region will be even lower when accounting for particle losses in head airways. Thus, the health concern from inhaling nanoparticles remains mainly for large airways in the TB region. Predicted deposition fractions were in good agreement with available measurements in the literature for total deposition. Some differences were observed when predicted regional depositions were compared with reported values based on total deposition measurements. The differences may in part be explained by the uncertainties in the way measurement-based regional deposition values were derived.

REFERENCES

Anjilvel, S., and Asgharian, B. 1995. A multiple-path model of particle deposition in the rat lung. *Fundam. Appl. Toxicol.* 28:41–50.

Asgharian, B.,Hofmann, W., and Bergmann, R. 2001. Particle deposition in a multiple-path model of the human lung. *Aerosol Sci. Technol.* 34:332–339.

Asgharian, B., Ménache, M. G., and Miller, F. J. 2004. Modeling age-related particle deposition in humans. *J. Aerosol Med.* 17:213–224.

Chang, H.-K., and Farhi, L. E. 1973. On mathematical analysis of gas transport in the lung. *Respir. Physiol.* 18:370–385.

Cohen, B. S., and Asgharian, B. 1990. Deposition of ultrafine particles in the upper airways: An empirical analysis. *J. Aerosol Sci.* 21:789–797.

Cohen, B. S., Sussman, R. G., and Lippmann, M. (1990). Ultrafine particle deposition in a human tracheobronchial cast. *Aerosol Sci. Technol.* 12:1082–1091.

Darquenne, C., and Paiva, M. 1994. One-dimensional simulation of aerosol transport and deposition in the human lung. *J. Appl. Physiol.* 77:2889–2898.

Darquenne, C., and Prisk, G. M. 2004. Effect of small flow reversals on aerosol mixing in the alveolar region of the human lung. *J. Appl. Physiol.* 97:2083–2089.

Darquenne C., Brand, P., Heyder, J., and Paiva, M. 1977. Aerosol dispersion in human lung: Comparison between numerical simulations and experiments for bolus tests. *J. Appl. Physiol.* 83:966–974.

Davidson, M. R. 1981. Further consideration in a theoretical description of gas transport in lung airways. *Bull. Math Biol.* 43:517–548.

Edwards, D. 1994. A general theory of the macrotransport of nondepositing particles in the lung by convective dispersion. *J. Aerosol Sci.* 25:543–565.

Egan, M. J., Nixon, W., Robinson, N. I., James, A. C., and Phalen, R. F. 1989. Inhaled aerosol transport and deposition calculations for the ICRP Task Group. *J. Aerosol Sci.* 20:1305–1308.

Ferin, J., and Oberdörster, G. 1992. Pulmonary retention of ultrafine and fine particles in rats. *Am. J. Respir. Cell Mol. Biol.* 6:535–542.

Hashish, A. H. 1992. Selective deposition of pulsed aerosols in the human lung. *J. Aerosol Sci.* 23:S473–S476.

Henry, F. S., and Tsuda, A. 2002. Kinematic irreversible acinar flow: A departure from classical dispersive aerosol transport theories. *J. Appl. Physiol.* 92:835–845.

Henry, F. S., Butler, J. P., and Tsuda, A. 1999. Stretch-and-fold flow and aerosol mixing in the acinus. *Am. J. Respir. Crit. Care Med.* 159:A615–A615.

Heyder, J., Gebhart, G., Rudolf, C. F., and Stahlhofen, W. 1986. Deposition of particles in the human respiratory tract in the size range 0.005–15 μm. *J. Aerosol Sci.* 17:811–825.

Hofmann, W., and Koblinger, L. 1990. Monte Carlo modeling of Aerosol Deposition in human lungs. Part II: Deposition fractions and their sensitivity to parameter variations. *J. Aerosol Sci.* 21:675–688.

Hofmann, W., Koblinger, L., Brand, P., Ferron, G., and Heyder, J. 1994. The effect of convective mixing on particle transport in the human respiratory tract. *Ann. Occup. Hyg.* 38(Suppl. 1):167–174.

International Commission on Radiological Protection. 1994. *Human respiratory tract model for radiological protection*. Publication 66, Pergamon Press, Oxford, United Kingdom. *Ann. ICRP* 24:272.

Jaques, P. A., and Kim, C. S. 2000. Measurement of total lung deposition of inhaled ultrafine particles in healthy men and women. *Inhal. Toxicol.* 12:715–731.

Johnston, C. J., Finkelstein, J. N., Mercer, P., Corson, N., Gelein, R., and Oberdörster, G. 2000. Pulmonary effects induced by ultrafine PTEF particles. *Toxicol. Appl. Pharmacol.* 168:208–215.

Kim, C. S., and Jaques, P. A. 2000. Respiratory dose of inhaled ultrafine particles in healthy adults. *Philos. Trans. R. Soc. Lond. A* 358:2693–2705.

Koblinger, L., and Hofmann, W. 1985. Analysis of human lung morphometric data for stochastic aerosol deposition calculations. *Phys. Med. Biol.* 30:541–556.

Koblinger, L., and Hofmann, W. 1990. Monte Carlo modeling of aerosol deposition in human lungs. Part I: Simulation of particle transport in a stochastic lung structure. *J. Aerosol Sci.* 21(5):661–674.

Lee, D. Y., and Lee, J. W. 2001. Dispersion during exhalation of an aerosol bolus in a double bifurcation. *J. Aerosol Sci.* 32:805–815.

Lee, J. W., Lee, D. Y., and Kim, W. S. 2000. Dispersion of an aerosol bolus in a double bifurcation.*J. Aerosol Sci.* 31:491–505.

Makulova, I. D. 1965. The clinical picture in acute perfluoroisbutylene poisoning. *Gig. Tr. Prof. Zabol.* 9:20–23.

Maynard, A. D., Baron, P. A., Foley, M., Shedova, A. A., Kisin, E. R., and Castranova, V. 2004. Exposure to carbon nanotube material: aerosol release during the handling of unrefined single-walled carbon nanotube material. *J. Toxicol. Environ. Health A* 67:87–107.

Miller, F. J., Overton, J. H., Jaskot, R. H., and Menzel, D. B. 1985. A model of regional uptake of gaseous pollutants in the lung. *Toxicol. Appl. Pharmacol.* 79:11–27.

National Council on Radiological Protection and Measurements. 1997. *Deposition, retention and dosimetry of inhaled radioactive substances*. NCRP Report 125. Bethesda, MD: NCRP.

Nixon, W., and Egan, M. J. 1987. Modeling study of regional deposition of inhaled aerosols with special reference to effects of ventilation asymmetry. *J. Aerosol Sci.* 18:563–579.

Oberdörster, G., Ferin, J., Gelein, R., Soderholm, S. C., and Finkelstein, J. N. 1992. Role of the alveolar macrophage in lung injury: Studies with ultrafine particles. *Environ. Health Perspect.* 97:193–197.

Oberdörster, G., Gelein, R. M., Ferin, J., and Weiss, B. 1995. Association of particulate air pollution and acute mortality: involvement of ultrafine particles. *Inhal. Toxicol.* 7:111–124.

Overton, J. H. 2001. Dosimetry modeling of highly soluble reactive gases in the respiratory tract. *Inhal. Toxicol.* 13:347–357.

Overton, J. H., Kimbell, J. S., and Miller, F. J. 2001. Dosimetry modeling of inhaled formaldehyde: the human respiratory tract. *Toxicol. Sci.* 64:122–134.

Pack, A., Hooper, M. B., Nixon, W., and Taylor, J. C. 1977. A computational model of pulmonary gas transport incorporating effective diffusion. *Respir. Physiol.* 29:101–124.

Peters, A., Wichmann, H. E., Tuch, T., Heinrich, J., and Heyder, J. 1997. Respiratory effects are associated with the number of ultrafine particles. *Am J. Respir. Crit. Care Med.* 155:1376– 1383.

Raabe, O. G., Yeh, H. C., Schum, G. M., and Phalen, R. F. (1976). Tracheobronchial geometry: human, dog, rat, hamster, Report LF-53. Lovelace Foundation, Albuquerque, New Mexico.

Riesenfeld, E., Chalupa, D., Gibb, F. R., Oberdörster, G., Gelein, R., Morrow, P. E., Utell, M. J., and Frampton, M. W. 2000. Ultrafine particle concentrations in a hospital. *Inhal. Toxicol.* 12(Suppl. 2):83–94.

Rosenstock, L., and Cullen, M. R. 1986. *Clinical occupational medicine*, pp. 28, 232. Philadelphia, PA: Saunders.

Rudolf, G., Gebhart, J., Heyder, J., Schiller, C. F., and Stahlhofen, W. 1986. An empirical formula describing aerosol deposition in man for any particle size. *J. Aerosol Sci.* 17:350–355.

Rudolf, G., Kobrich, R., and Stahlhofen, W. 1990. Modeling and algebraic formulation of regional aerosol deposition in man. *J. Aerosol Sci.* 21(Suppl. 1):S403–S406.

Scherer, P. W., Shendalman, L. H., and Greene, N. M. 1972. Simultaneous diffusion and convection in single breath lung washout. *Bull. Math. Biophys.* 34:393–412.

Scherer, P. W., Shendalman, L. H., Green, N. M., and Bouhuys, A. 1975. Measurements of axial diffusivity in a model of the bronchial airways. *J. Appl. Physiol.* 38:719–723.

Schiller, C. F., Gebhart, J., Heyder, J., Rudolf, G., and Stahlhofen, W. 1988. Deposition of monodisperse insoluble aerosol particles in the 0.005 to 0.2 μm size range within the human respiratory tract. *Ann. Occup. Hyg.* 32:41–49.

Tan, C. W., and Hsu, C.-J. 1971. Diffusion of aerosols in laminar flow in a cylindrical tube. *J. Aerosl Sci.* 2:117–124.

Taulbee, D. B., and Yu, C. P. 1975. A Theory of aerosol deposition in the human respiratory tract. *J. Appl. Physiol.* 38:77–84.

Taulbee, D. B., Yu, C. P., and Heyder, J. 1978. Aerosol transport in the human lung from analysis of single breaths. *J. Appl. Physiol. Respirat. Environ.* 44:803–812.

Tawhai, M. H., and Hunter, P. J. 2001. Characterizing respiratory airway gas mixing using a lumped parameter model of the pulmonary acinus. *Respir. Physiol.* 127:241–248.

Tsuda, A., Henry, F. S., and Butler, J. P. 1995. Chaotic mixing of alveolated duct flow in rhythmically expanding pulmonary acinus. *J. Appl. Physiol.* 79:1055–1063.

Tsuda, A., Otani, Y., and Butler, J. P. 1999. Acinar flow irreversibility caused by perturbations in reversible alveolar wall motion. *J. Appl. Phsiol.* 86:977–984.

Tu, K. W., and Knutson, E. O. 1984. Total deposition of ultrafine hydrophobic and hygroscopic aerosols in the human respiratory system.*Aerosol Sci. Technol.* 3:453–465.

Utell, M. J., and Frampton, M. W. 2000. Who is susceptible to particulate matter and why? *Inhal. Toxicol.* 12(Suppl. 1):37–40.

Yu, C. P. 1975. On equation of gas transport in the lung. *Respir. Physiol.* 23:257–266.

Yu, C. P. 1978a. Exact analysis of aerosol deposition during steady state breathing. *Powder Technol.* 21:55–62.

Yu, C. P. 1978b. A two-compartment theory of aerosol deposition in human lung airways. *Bull. Math. Biol.* 40:693–706.